

Cite this: *Phys. Chem. Chem. Phys.*, 2020, 22, 25827

π -Orbital Yin–Yang Kagome bands in anilato-based metal–organic frameworks†

Xiaojuan Ni,  Yinong Zhou, Gurjyot Sethi and Feng Liu*

π -Orbital bonding plays an important role not only in traditional molecular science and solid-state chemistry but also in modern quantum physics and materials, such as the relativistic Dirac states formed by bonding and antibonding π -bands in graphene. Here, we disclose an interesting manifestation of π -orbitals in forming the Yin–Yang Kagome bands, which host potentially a range of exotic quantum phenomena. Based on first-principles calculations and tight-binding orbital analyses, we show that the frontier π_2 - and π_3 -orbitals in anilato-based metal–organic frameworks form concurrently a conduction and valence set of Kagome bands, respectively, but with opposite signs of lattice hopping to constitute a pair of enantiomorphic Yin and Yang Kagome bands, as recently proposed in a diatomic Kagome lattice. The twisted configuration of neighboring benzene-derived organic ligands bridged by an octahedrally O-coordinated metal ion is found to play a critical role in creating the opposite sign of lattice hopping for the π_2 - versus π_3 -orbitals. Our finding affords a new material platform to study π -orbital originated quantum chemistry and physics.

Received 24th July 2020,
Accepted 12th October 2020

DOI: 10.1039/d0cp03941a

rsc.li/pccp

Introduction

Chemical bond analysis, such as the Lewis theory of bonding^{1–3} and molecular orbital (MO) theory,^{4–6} is of major importance in the traditional molecular chemistry as well as modern quantum physics and materials.^{7,8} One distinguished example is π -orbital bonding,^{9,10} such as the frontier π -orbitals in cycloaddition reactions,^{11–14} and the π -conjugation in covalent organic frameworks^{15–18} and metal–organic frameworks (MOFs).^{19,20} A star quantum material, graphene that displays fascinating relativistic Dirac states, is notably formed by bonding and antibonding π -bands.^{21,22} The π -orbitals are originally discovered in benzene,^{4,23–27} manifesting the resonant six p_z orbitals, as illustrated in Fig. 1(a) and (b), which differ distinctively from typical covalent or ionic bonds. They exist ubiquitously in numerous benzene derivatives, such as the anilato-based ligands, the chloranilic acid (CLA, C₆H₂Cl₂O₄),^{28–31} which is of our interest here. As shown in Fig. 1(c), because of the addition of halogen and oxygen atoms, CLA has a lower symmetry to lift the energy degeneracy between the π_2 - and π_3 -orbitals, and also the number of valence electrons locates the “Fermi level” in between these two orbitals so that they become the lowest unoccupied MO (LUMO) and the highest occupied MO (HOMO), respectively.^{32,33} Details on the composition

and properties of π_2 - and π_3 -orbitals in CLA and also in metal ion-bonded CLAs are shown in Fig. S1 in ESI.†

On the other hand, it is well-known that both lattice and orbital symmetries play important roles in giving rise to exotic band structures that host novel quantum states.³⁴ For example, consider single s -orbital hopping, *i.e.* of simplest orbital symmetry, Dirac bands and topological flat bands (FBs) are formed, respectively in a hexagonal^{35–37} and Kagome lattice,^{37–44} due to solely lattice symmetry; while both such bands can also be formed in a hexagonal lattice with (p_x , p_y)-orbital hopping, due to the additional orbital symmetry.^{45–49} Very recently, an

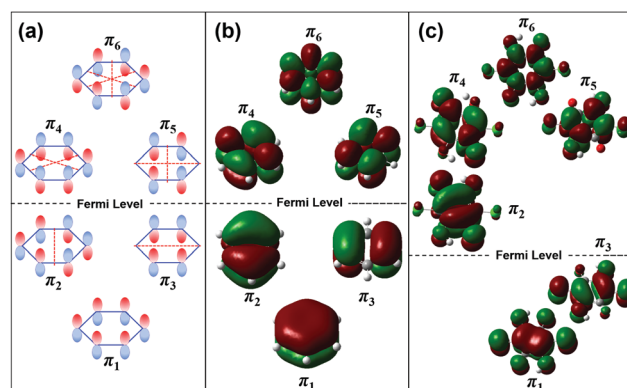


Fig. 1 (a) Schematic illustration of 6 π -orbitals in benzene. The red dashed line indicates the nodal plane. Calculated orbital distribution of 6 π -orbitals by Gaussian: (b) in benzene, and (c) in chloranilic acid (C₆H₂Cl₂O₄). Green and red indicate the positive and negative sign of lobes, respectively.

Department of Materials Science and Engineering, University of Utah, Salt Lake, Utah 84112, USA. E-mail: fliu@eng.utah.edu

† Electronic supplementary information (ESI) available. See DOI: 10.1039/d0cp03941a

interesting diatomic single-orbital Kagome lattice model has been proposed to exhibit the so-called Yin–Yang Kagome bands, which consist of two sets of enantiomorphic Kagome bands,⁵⁰ particularly two FBs of opposite Chern numbers separated by an energy gap. It has been further theoretically shown that photoexcitation between the two FBs is chiral selective, leading to excited quantum Hall effect and giant circular dichroism (CD).⁵⁰ For example, two flatronic devices of topological photodetectors in a photovoltaic cell and circularly polarized lasers in a heterojunction diode have been proposed based on the flat-CD mechanism.⁵¹

However, there are some intriguing lattice hopping conditions required to realize the Yin–Yang Kagome bands in a diatomic Kagome lattice. For example, the longer-distance cross-hopping between two sub-Kagome lattices needs to be larger than the shorter-distance interatomic hopping.⁵⁰ Such unusual hopping conditions make the suitable diatomic-Kagome-lattice materials rather limited. Here, we disclose a new scheme to realize Yin–Yang Kagome bands in a “monomolecular”, instead of diatomic, Kagome lattice with two orbitals per lattice site, by exploiting orbital symmetry in addition to lattice symmetry. In particular, the resulting Yin–Yang Kagome bands represent another intriguing manifestation of π -orbitals. Based on first-principles calculations and tight-binding orbital analyses, we show that the frontier π_2 - and π_3 -orbitals in the anilato-based MOFs $M_2(C_6O_4X_2)_3$ with $M = \text{Al, Ga, In}$ and $X = \text{H, F, Cl, Br, I, OH, CN}$ form, strikingly, a pair of enantiomorphic Yin–Yang Kagome bands. The TB model analysis further reveals that the π_2 - and π_3 -orbitals sit on the same Kagome lattice site and hop concurrently but with an opposite sign of lattice hopping, leading to the formation of Yin and Yang Kagome bands, respectively. In particular, the twisted configuration of the neighboring benzene-derived organic ligands, formed by a metal ion bonding octahedrally with six oxygen atoms, is found to be vital to create the opposite sign of lattice hopping for π_2 - versus π_3 -orbitals. Furthermore, the gap between the two FBs can be tuned by substituting organic ligands of different electronegativities.

Results and discussion

The anilato-based coordination frameworks have a great variety, ranging from isolated oligomers to extended one dimensional (1D), 2D, and 3D MOFs,^{52–57} showing the peculiar magnetic, electronic, and topological properties.^{58–62} Especially, the 2D anilato-based MOFs with a chemical formula of $M_2(C_6O_4X_2)_3$, as shown in Fig. 2(a), have been extensively studied in experiments with $M =$ metal ions ($\text{Mg},^{63} \text{Al},^{64} \text{Ti},^{61} \text{V},^{61} \text{Cr},^{61} \text{Mn},^{63,65} \text{Fe},^{58–60,63,66–69} \text{Co},^{56,63} \text{Ni},^{63} \text{Cu},^{56} \text{Zn},^{56,60,63,68} \text{Y},^{70} \text{Cd},^{56,63,65}$ and $\text{Ln}^{71–74}$), and X is the substituent. Here, we choose $\text{Al}_2(\text{C}_6\text{O}_4\text{Cl}_2)_3$ as a prototype for our case study of π -orbital Yin–Yang Kagome bands. The lattice constant of $\text{Al}_2(\text{C}_6\text{O}_4\text{Cl}_2)_3$ is 13.16 Å, which is comparable to 13.135 Å obtained in experiments.⁶⁴ As the Al ion is octahedrally bonded with six oxygen atoms, three neighboring organic ligands are twisted from each other with

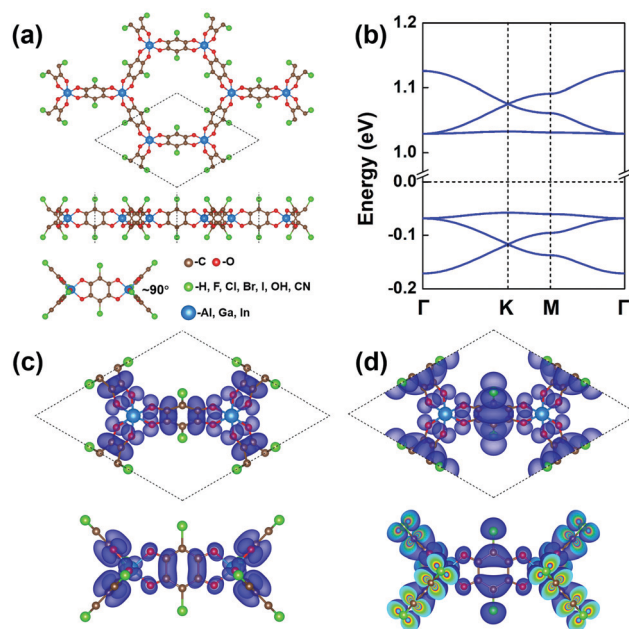


Fig. 2 (a) Top and side views of the crystal structure of anilato-based MOFs $M_2(C_6O_4X_2)_3$. The lower panel represents the dihedral angle between two neighboring organic ligands (taking the carbon-ring as the basal plane), which is $\sim 90^\circ$. (b) DFT band structure of $\text{Al}_2(\text{C}_6\text{O}_4\text{Cl}_2)_3$. (c and d) Are the top and auxiliary views of partial charge distribution of conduction and valence Kagome bands, respectively. The dashed rhombus indicates the unit cell.

a dihedral angle (DA) of $\sim 90^\circ$, with each carbon-ring lying in the x - y , y - z and x - z basal planes. *Ab initio* molecular dynamics simulation (Fig. S2 in ESI†) has been carried out to confirm the structural stability of monolayer $\text{Al}_2(\text{C}_6\text{O}_4\text{Cl}_2)_3$. The derived interlayer binding energy of $\text{Al}_2(\text{C}_6\text{O}_4\text{Cl}_2)_3$ indicates a high feasibility of exfoliating layered anilato-based MOFs into 2D layers, similar to other 2D materials (Fig. S3 in ESI†).

Fig. 2(b) shows two sets of enantiomorphic Yin–Yang Kagome bands obtained from density functional theory (DFT) calculations, with the Fermi level located in between them and far away from other bands (see Fig. S4 in ESI†). The partial charge distribution of conduction and valence Kagome bands is shown in Fig. 2(c) and (d), which are predominantly contributed from C–O and C–Cl orbitals, respectively, with no contribution from Al (see Fig. S5 in ESI† for details). After considering spin–orbital coupling (SOC), there are small gaps of 1.50 and 0.70 meV for conduction Kagome bands, and 0.41 and 0.16 meV for valence Kagome bands opened at Γ and K points, respectively (Fig. S6 in the ESI†). The nontrivial topology of the enantiomorphic Kagome bands in $\text{Al}_2(\text{C}_6\text{O}_4\text{Cl}_2)_3$ has been confirmed by calculating the edge states and Z_2 number with the maximally localized Wannier functions (Fig. S7 and S8 in ESI†).^{75–77}

To better understand the electronic and topological properties of $\text{Al}_2(\text{C}_6\text{O}_4\text{Cl}_2)_3$, TB model analyses are performed. The partial charge distribution of conduction and valence Kagome bands is found to retain the features of π_2 - and π_3 -orbitals in CLA, respectively. Note that there is a phase change of π -orbitals in neighboring ligands around each Al ion (Fig. S1 in ESI†), which

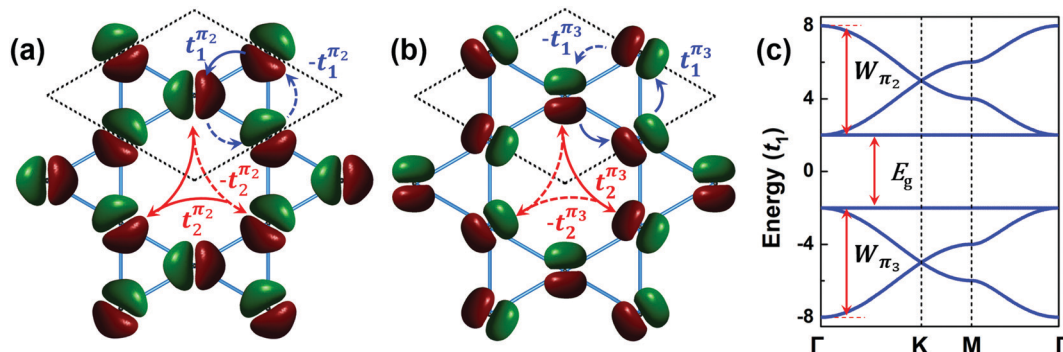


Fig. 3 Illustrations of the TB model consisting of (a) π_2 - and (b) π_3 -orbitals in a Kagome lattice. The dashed rhombus indicates the unit cell. t_1 and t_2 represent the NN and 2NN hopping. The negative sign indicates the hopping between two π orbitals with opposite signs of lobes facing each other. Green and red colors indicate the positive and negative sign of lobes, respectively. (c) The ideal enantiomorphic Kagome bands obtained from the TB model with $t_1, t_2 = 0, \varepsilon_{\pi_2} = 4|t_1|$, and $\varepsilon_{\pi_3} = -4|t_1|$. The band gap between the two FBs $E_g = |\Delta\varepsilon - 2(t_1^{\pi_2} + t_1^{\pi_3})|$, bandwidth $W_{\pi_2} = 6|t_1^{\pi_2}|$, and $W_{\pi_3} = 6|t_1^{\pi_3}|$. Here, $t_1^{\pi_2} = t_1^{\pi_3} = t_1, \Delta\varepsilon = \varepsilon_{\pi_2} - \varepsilon_{\pi_3}$.

is also adopted in the TB model. The illustrations of the TB model with π_2 - and π_3 -orbitals in a Kagome lattice are shown in Fig. 3(a) and (b), respectively. The TB Hamiltonian is defined as,

$$H = \sum_i \varepsilon_i c_i^\dagger c_i + \sum_{\langle i,j \rangle} t_1 c_i^\dagger c_j + \sum_{\langle\langle i,j \rangle\rangle} t_2 c_i^\dagger c_j + i\lambda_{\text{SO}} \sum_{\langle\langle i,j \rangle\rangle} \left(\frac{\vec{d}_{jk}}{|\vec{d}_{jk}|} \times \frac{\vec{d}_{ki}}{|\vec{d}_{ki}|} \right) c_i^\dagger \sigma_z c_j + hc,$$

where ε_i is the on-site energy, c_i^\dagger and c_i are the creation and annihilation operators of an electron on site i , respectively. t_1 and t_2 represent the hopping between the nearest-neighbor (NN) $\langle i,j \rangle$ and the second nearest-neighbor (2NN) $\langle\langle i,j \rangle\rangle$ sites, respectively, λ_{SO} is the strength of spin-orbital coupling (SOC), σ_z is the z-component of Pauli matrices, and \vec{d}_{ki} is the vector from site i to site k . The negative sign in front of hopping t indicates the hopping between two π -orbitals with opposite signs of lobes facing each other. As a result, the lattice hopping of π_2 - and π_3 -orbitals is effectively performed with an opposite sign. The band structure obtained from the TB model, with a gap between the two FBs $E_g = |\Delta\varepsilon - 2(t_1^{\pi_2} + t_1^{\pi_3})|$, is shown in Fig. 3(c). For simplicity, we set $t_1^{\pi_2} = t_1^{\pi_3}$, which in principle can be different but without changing the key features of the overall band structure. More details of the TB model are provided in the ESI.†

Al ions are preferred for octahedral coordination with six oxygen atoms of three deprotonated organic ligands in a highly symmetrical configuration, resulting in an orthogonal orbital orientation between neighboring ligands. This orthogonality turns out to be critical in forming the FBs. We have analysed the DA dependence of FB, by artificially tuning the DA from 93° , to 75° , and to 67° , to gradually decrease the orthogonality. Both DFT and TB calculations show that with the decreasing DA, the two FBs are no longer flat and meantime the bandwidth of both conduction and valence Kagome bands increases, as shown in Fig. S9 and Table S1 in ESI.† It is known that the 2NN interaction affects the flatness of FB in the Kagome lattice.^{43,78} Since the orthogonal neighboring π -orbitals have

the smallest hopping, rotating away from the orthogonal configuration will increase the 2NN hopping t_2 , and hence deteriorate the flatness of FBs.

Considering SOC in the TB model, the topological invariant Z_2 number has been calculated by checking the parity of occupied bands at time-reversal invariant momenta (Table S2 and Fig. S10 in ESI.†).⁷⁹ For each spin channel, the two FBs have opposite spin Chern numbers to realize the Yin–Yang Kagome bands, as shown in the original lattice model.⁵⁰

Next, we demonstrate the band gap between two FBs which can change with the substituent of X since the band gap plays a crucial role in the optoelectronic applications.^{80–83} The semi-local approximations to the exchange–correlation potentials of Perdew, Burke, and Ernzerhof (PBE)^{84,85} are used first in the DFT calculations. However, it is known to underestimate the band gap.^{86–88} Therefore, the screened hybrid functional of Heyd, Scuseria, and Ernzerhof (HSE)⁸⁹ (Fig. S11 in ESI.†) is also used to correct the band gap of PBE, as shown in Fig. 4. Except for the different gap sizes, the overall trend of band gap, changing with the substituents of different electronegativity, remains the same. $\text{Al}_2(\text{C}_6\text{O}_4\text{X}_2)_3$ with the substituent of X = H in ligands has the largest gap (2.77 eV), which is followed by CN (2.42 eV), and OH (2.32 eV). The halogen substituents lead to a relatively small gap size, from F of 2.26 eV to I of 1.99 eV. The origin of the gap difference in the MOFs is found to directly correlate with the HOMO–LUMO gap between the π_2 - and π_3 -orbitals (Fig. S12 in ESI.†) in the corresponding organic ligand,^{17,90–92} which form respectively the valence and conduction bands as shown above. In addition, the band gap of $\text{Al}_2(\text{C}_6\text{O}_4\text{Cl}_2)_3$ decreases slightly with the increasing strain without affecting the Yin–Yang Kagome bands (Fig. S13 in ESI.†).

Lastly, we explored other members in the family of anilato-based MOFs $\text{M}_2(\text{C}_6\text{O}_4\text{X}_2)_3$ with X = H, CN, OH, F, Cl, Br, and I, and M = Al, Ga, and In, which are found to also host the enantiomorphic Yin–Yang Kagome bands formed by π -orbitals (Fig. S14 and S15, ESI.†). The band gap between two FBs does not have a strong dependence on metal ions (Fig. S16, ESI.†). MOFs with Ga and In have the same trend of $E_{g,\text{FB}}$ with respect to different organic ligand substituents as that in $\text{Al}_2(\text{C}_6\text{O}_4\text{X}_2)_3$.

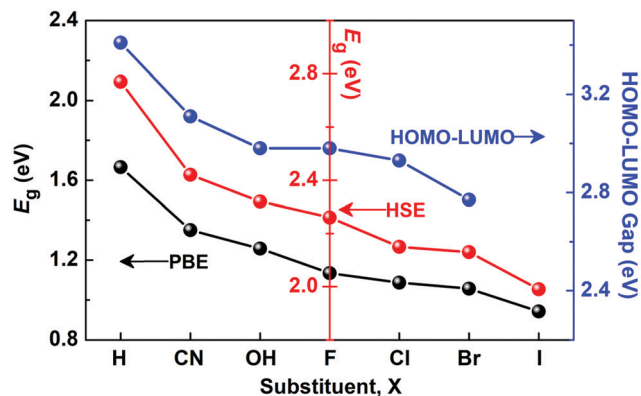


Fig. 4 Energy gap for different substituents X in $\text{Al}_2(\text{C}_6\text{O}_4\text{X}_2)_3$ calculated in the framework of PBE (black), HSE06 (red), and HOMO-LUMO gap in molecules of $\text{C}_6\text{O}_4\text{X}_2\text{H}_2$ (blue).

Conclusions

In summary, dual frontier π -orbitals in anilato-based MOFs have been found to form intriguing enantiomeric Yin–Yang Kagome bands, which are based on an orbital-symmetry mechanism different from the original diatomic Kagome model based on lattice symmetry. In particular, the resulting gap size between two flat bands is determined by the HOMO–LUMO gap of original molecular orbitals and hence be readily tuned by the choice of molecules, while the same gap in the diatomic Kagome lattice depends on the interatomic interaction which is much harder to tune. The twisted orthogonal configuration of neighboring ligands bridged by an octahedrally O-coordinated metal ion is critical, on one hand, to create the opposite sign of lattice hopping for the two frontier π -orbitals, and on the other hand, to ensure the flatness of flat bands. Our finding not only enriches the fundamental chemistry and physics of π -orbitals in association with Yin–Yang Kagome bands, but also significantly expands the pool of materials hosting enantiomeric Kagome bands. Broadly, it provides a new platform to study π -orbital originated quantum chemistry and physics.

Conflicts of interest

There are no conflicts to declare.

Acknowledgements

This work is supported by the U.S. Department of Energy-Basic Energy Sciences (Grant No. DE-FG02-04ER46148). We acknowledge NERSC and CHPC at the University of Utah for providing the computing resources.

References

- 1 G. N. Lewis, *J. Am. Chem. Soc.*, 1913, **35**, 1448–1455.
- 2 G. N. Lewis, *J. Am. Chem. Soc.*, 1916, **38**, 762–785.

- 3 G. N. Lewis, *Valence and the structure of atoms and molecules*, 1923.
- 4 I. Fleming, *Molecular orbitals and organic chemical reactions*, Student edn, 2011.
- 5 I. Fleming, *Frontier orbitals and organic chemical reactions*, 1977.
- 6 K. Fukui, *Acc. Chem. Res.*, 1971, **4**, 57–64.
- 7 S. Shaik, *J. Comput. Chem.*, 2007, **28**, 51–61.
- 8 G. Frenking and S. Shaik, *The Chemical Bond: Fundamental Aspects of Chemical Bonding*, Wiley Blackwell, 2014, vol. 9783527333.
- 9 F. R. Wagner, V. Bezugly, M. Kohout and Y. Grin, *Chem. – Eur. J.*, 2007, **13**, 5724–5741.
- 10 L. Pauling, *J. Am. Chem. Soc.*, 1931, **53**, 1367–1400.
- 11 C. A. Caputo, J. D. Guo, S. Nagase, J. C. Fettinger and P. P. Power, *J. Am. Chem. Soc.*, 2012, **134**, 7155–7164.
- 12 Y. Peng, B. D. Ellis, X. Wang, J. C. Fettinger and P. P. Power, *Science*, 2009, **325**, 1668–1670.
- 13 M. Lautens, W. Tam, J. C. Lautens, L. G. Edwards, C. M. Crudden and A. C. Smith, *J. Am. Chem. Soc.*, 1995, **117**, 6863–6879.
- 14 K. Fukui, *Angew. Chem., Int. Ed. Engl.*, 1982, **21**, 801–809.
- 15 J. J. Adjizian, P. Briddon, B. Humbert, J. L. Duvail, P. Wagner, C. Adda and C. Ewels, *Nat. Commun.*, 2014, **5**, 5842.
- 16 S. Kandambeth, K. Dey and R. Banerjee, *J. Am. Chem. Soc.*, 2019, **141**, 1807–1822.
- 17 Y. Jing and T. Heine, *J. Am. Chem. Soc.*, 2019, **141**, 743–747.
- 18 S. Thomas, H. Li, C. Zhong, M. Matsumoto, W. R. Dichtel and J. L. Bredas, *Chem. Mater.*, 2019, **31**, 3051–3065.
- 19 X. Sun, K.-H. Wu, R. Sakamoto, T. Kusamoto, H. Maeda, X. Ni, W. Jiang, F. Liu, S. Sasaki, H. Masunagai and H. Nishihara, *Chem. Sci.*, 2017, **8**, 8078–8085.
- 20 T. Kambe, R. Sakamoto, T. Kusamoto, T. Pal, N. Fukui, K. Hoshiko, T. Shimojima, Z. Wang, T. Hirahara, K. Ishizaka, S. Hasegawa, F. Liu and H. Nishihara, *J. Am. Chem. Soc.*, 2014, **136**, 14357–14360.
- 21 T. Ohta, A. Bostwick, T. Seyller, K. Horn and E. Rotenberg, *Science*, 2006, **313**, 951–954.
- 22 J. Jung and A. H. Macdonald, *Phys. Rev. B: Condens. Matter Mater. Phys.*, 2013, **87**, 195450.
- 23 J. W. Moskowitz and M. P. Barnett, *J. Chem. Phys.*, 1963, **39**, 1557–1560.
- 24 J. M. Schulman and J. W. Moskowitz, *J. Chem. Phys.*, 1965, **43**, 3287–3290.
- 25 W. C. Ermler, R. S. Mulliken and E. Clement, *J. Am. Chem. Soc.*, 1976, **98**, 388–394.
- 26 P. C. Hiberty, D. Danovich, A. Shurki and S. Shaik, *J. Am. Chem. Soc.*, 1995, **117**, 7760–7768.
- 27 M. Öncan, F. Koç, M. Sahin and K. Köksal, *Int. J. Mod. Phys. B*, 2017, **31**, 1750095.
- 28 H. Hettegger, H. Amer, N. S. Zwirchmayr, M. Bacher, T. Hosoya, A. Potthast and T. Rosenau, *Cellulose*, 2019, **26**, 185–204.
- 29 V. Milašinović and K. Molčanov, *Croat. Chem. Acta*, 2018, **91**, 177–186.

- 30 K. Molčanov, M. Jurić and B. Kojić-Prodić, *Dalton Trans.*, 2013, **42**, 15756–15765.
- 31 K. Molčanov, M. Jurić and B. Kojić-Prodić, *Dalton Trans.*, 2014, **43**, 7208–7218.
- 32 K. M. Al-Ahmary, S. M. Soliman, R. A. Mekheimer, M. M. Habeeb and M. S. Alenezi, *J. Mol. Liq.*, 2017, **231**, 602–619.
- 33 K. M. Al-Ahmary, M. M. Habeeb and A. H. Al-Obidan, *Spectrochim. Acta, Part A*, 2018, **196**, 247–255.
- 34 Z. F. Wang, K. Jin and F. Liu, *Wiley Interdiscip. Rev.: Comput. Mol. Sci.*, 2017, **7**, e1304.
- 35 C. L. Kane and E. J. Mele, *Phys. Rev. Lett.*, 2005, **95**, 146802.
- 36 C. L. Kane and E. J. Mele, *Phys. Rev. Lett.*, 2005, **95**, 226801.
- 37 M. A. Springer, T. J. Liu, A. Kuc and T. Heine, *Chem. Soc. Rev.*, 2020, **49**, 2007–2019.
- 38 K. Ohgushi, S. Murakami and N. Nagaosa, *Phys. Rev. B: Condens. Matter Mater. Phys.*, 2000, **62**, R6065–R6068.
- 39 Z. Liu, F. Liu and Y. S. Wu, *Chin. Phys. B*, 2014, **23**, 077308.
- 40 C. C. Lee, A. Fleurence, Y. Yamada-Takamura and T. Ozaki, *Phys. Rev. B*, 2019, **100**, 045150.
- 41 W. Jiang, M. Kang, H. Huang, H. Xu, T. Low and F. Liu, *Phys. Rev. B*, 2019, **99**, 125131.
- 42 S. Zhang, M. Kang, H. Huang, W. Jiang, X. Ni, L. Kang, S. Zhang, H. Xu, Z. Liu and F. Liu, *Phys. Rev. B*, 2019, **99**, 100404R.
- 43 E. Tang, J. W. Mei and X. G. Wen, *Phys. Rev. Lett.*, 2011, **106**, 236802.
- 44 S. A. Parameswaran, I. Kimchi, A. M. Turner, D. M. Stamper-Kurn and A. Vishwanath, *Phys. Rev. Lett.*, 2013, **110**, 125301.
- 45 M. Zhou, W. Ming, Z. Liu, Z. Wang, Y. Yao and F. Liu, *Sci. Rep.*, 2014, **4**, 7102.
- 46 M. Zhou, W. Ming, Z. Liu, Z. Wang, P. Li and F. Liu, *Proc. Natl. Acad. Sci. U. S. A.*, 2014, **111**, 14378–14381.
- 47 X. Ni, H. Huang and F. Liu, *Phys. Rev. B*, 2020, **101**, 125114.
- 48 F. Dominguez, B. Scharf, G. Li, J. Schäfer, R. Claessen, W. Hanke, R. Thomale and E. M. Hankiewicz, *Phys. Rev. B*, 2018, **98**, 161407R.
- 49 L. M. Canonico, T. G. Rappoport and R. B. Muniz, *Phys. Rev. Lett.*, 2019, **122**, 196601.
- 50 Y. Zhou, G. Sethi, H. Liu and F. Liu, 2019, arXiv:1908.03689.
- 51 Y. Zhou, G. Sethi, C. Zhang, X. Ni and F. Liu, *Phys. Rev. B*, 2020, **102**, 125115.
- 52 R. Spengler, J. Lange, H. Zimmermann, H. Burzclaff, P. G. Veltsistas and M. I. Karayannis, *Acta Crystallogr., Sect. B: Struct. Sci.*, 1995, **51**, 174–177.
- 53 K. S. Min, A. L. Rhinegold and J. S. Miller, *J. Am. Chem. Soc.*, 2006, **128**, 40–41.
- 54 S. Kitagawa and S. Kawata, *Coord. Chem. Rev.*, 2002, **224**, 11–34.
- 55 S. Benmansour, C. Vallés-García, P. Gómez-Claramunt, G. M. Espallargas and C. J. Gómez-García, *Inorg. Chem.*, 2015, **54**, 5410–5418.
- 56 T. T. Luo, Y. H. Liu, H. L. Tsai, C. C. Su, C. H. Ueng and K. L. Lu, *Eur. J. Inorg. Chem.*, 2004, 4253–4258.
- 57 M. Atzori, L. Marchiò, R. Clérac, A. Serpe, P. Deplano, N. Avarvari and M. L. Mercuri, *Cryst. Growth Des.*, 2014, **14**, 5938–5948.
- 58 M. Atzori, S. Benmansour, G. Mínguez Espallargas, M. Clemente-León, A. Abhervé, P. Gómez-Claramunt, E. Coronado, F. Artizzu, E. Sessini, P. Deplano, A. Serpe, M. L. Mercuri and C. J. Gómez García, *Inorg. Chem.*, 2013, **52**, 10031–10040.
- 59 I. R. Jeon, B. Negru, R. P. V. Duyne and T. D. Harris, *J. Am. Chem. Soc.*, 2015, **137**, 15699–15702.
- 60 J. A. DeGayner, I. R. Jeon, L. Sun, M. Dincă and T. D. Harris, *J. Am. Chem. Soc.*, 2017, **139**, 4175–4184.
- 61 M. E. Ziebel, L. E. Darago and J. R. Long, *J. Am. Chem. Soc.*, 2018, **140**, 3040–3051.
- 62 X. Ni, W. Jiang, H. Huang, K. H. Jin and F. Liu, *Nanoscale*, 2018, **10**, 11901–11906.
- 63 C. J. Kingsbury, B. F. Abrahams, D. M. D. Alessandro, T. A. Hudson, R. Murase, R. Robson and K. F. White, *Cryst. Growth Des.*, 2017, **17**, 1465–1470.
- 64 S. Halis, A. K. Inge, N. Dehning, T. Weyrich, H. Reinsch and N. Stock, *Inorg. Chem.*, 2016, **55**, 7425–7431.
- 65 A. Weiss, E. Riegler and C. Robl, *Z. Naturforsch., B: J. Chem. Sci.*, 1986, **41**, 1501–1505.
- 66 G. V. Shilov, Z. K. Nikitina, N. S. Ovanesyan, S. M. Aldoshin and V. D. Makhaev, *Russ. Chem. Bull.*, 2011, **60**, 1209–1219.
- 67 S. Benmansour, P. Gómez-Claramunt, C. Vallés-García, G. M. Espallargas and C. J. G. García, *Cryst. Growth Des.*, 2016, **16**, 518–526.
- 68 C. J. Kingsbury, B. F. Abrahams, D. M. D'Alessandro, T. A. Hudson, R. Murase, R. Robson and K. F. White, *Cryst. Growth Des.*, 2017, **17**, 1465–1470.
- 69 S. Aldoshin, R. Academy, V. Makhaev, R. Academy and A. Mössbauer, *Russ. Chem. Bull.*, 2011, **60**, 1209–1219.
- 70 C. Robl, *Mater. Res. Bull.*, 1987, **22**, 1483–1491.
- 71 S. Benmansour, A. Hernández-Paredes and C. J. Gómez-García, *J. Coord. Chem.*, 2018, **71**, 845–863.
- 72 S. A. Sahadevan, N. Monni, A. Abhervé, G. Cosquer, M. Oggianu, G. Ennas, M. Yamashita, N. Avarvari and M. L. Mercuri, *Inorg. Chem.*, 2019, **58**, 13988–13998.
- 73 K. Bondaruk and C. Hua, *Cryst. Growth Des.*, 2019, **19**, 3338–3347.
- 74 S. Benmansour, I. Pérez-Herráez, G. López-Martínez and C. J. Gómez García, *Polyhedron*, 2017, **135**, 17–25.
- 75 A. A. Mostofi, J. R. Yates, Y. Lee, I. Souza, D. Vanderbilt and N. Marzari, *Comput. Phys. Commun.*, 2008, **178**, 685–699.
- 76 I. Souza, N. Marzari and D. Vanderbilt, *Phys. Rev. B: Condens. Matter Mater. Phys.*, 2002, **65**, 035109.
- 77 N. Marzari and D. Vanderbilt, *Phys. Rev. B: Condens. Matter Mater. Phys.*, 1997, **56**, 12847–12865.
- 78 T. Mizoguchi and M. Udagawa, *Phys. Rev. B*, 2019, **99**, 235118.
- 79 L. Fu and C. L. Kane, *Phys. Rev. B: Condens. Matter Mater. Phys.*, 2007, **76**, 045302.
- 80 C. Zhang, H. Huang, X. Ni, Y. Zhou, L. Kang, W. Jiang, H. Chen, J. Zhong and F. Liu, *Nanoscale*, 2018, **10**, 16759–16764.
- 81 N. Lu, H. Guo, L. Li, J. Dai, L. Wang, W. N. Mei, X. Wu and X. C. Zeng, *Nanoscale*, 2014, **6**, 2879–2886.
- 82 Y. Wang, P. T. Dickens, J. B. Varley, X. Ni, E. Lotubai, S. Sprawls, F. Liu, V. Lordi, S. Krishnamoorthy, S. Blair,

- K. G. Lynn, M. Scarpulla and B. Sensale-Rodriguez, *Sci. Rep.*, 2018, **8**, 18075.
- 83 Z. Liu, J. Wu, W. Duan, M. G. Lagally and F. Liu, *Phys. Rev. Lett.*, 2010, **105**, 016802.
- 84 J. P. Perdew, K. Burke and M. Ernzerhof, *Phys. Rev. Lett.*, 1997, **78**, 1396.
- 85 J. P. Perdew, K. Burke and M. Ernzerhof, *Phys. Rev. Lett.*, 1996, **77**, 3865–3868.
- 86 J. P. Perdew, *Int. J. Quantum Chem.*, 1985, **28**, 497–523.
- 87 M. Grüning, A. Marini and A. Rubio, *J. Chem. Phys.*, 2006, **124**, 154108.
- 88 J. P. Perdew and M. Levy, *Phys. Rev. Lett.*, 1983, **51**, 1884–1887.
- 89 A. V. Krukau, O. A. Vydrov, A. F. Izmaylov and G. E. Scuseria, *J. Chem. Phys.*, 2006, **125**, 224106.
- 90 X. P. Wu, L. Gagliardi and D. G. Truhlar, *J. Am. Chem. Soc.*, 2018, **140**, 7904–7912.
- 91 M. E. Foster, J. D. Azoulay, B. M. Wong and M. D. Allendorf, *Chem. Sci.*, 2014, **5**, 2081–2090.
- 92 H. Q. Pham, T. Mai, N. N. Pham-Tran, Y. Kawazoe, H. Mizuseki and D. Nguyen-Manh, *J. Phys. Chem. C*, 2014, **118**, 4567–4577.